Fletcher, Lyndsay (1997) Numerical simulations of coronal particle trapping. Astronomy and Astrophysics, 326 . pp. 1259-1267. ISSN 0004-6361

http://eprints.gla.ac.uk/91462/

Deposited on: 28 February 2014

Numerical simulations of coronal particle trapping

Lyndsay Fletcher

Solar System Division, ESA Space Science Department, ESTEC, Postbus 299, 2200 AG Noordwijk, The Netherlands

Abstract. In this paper the trapping of high energy particles in solar coronal loops is addressed. Using simulations, the time evolution of electrons and protons trapped in a magnetic bottle is calculated under various scattering conditions and the results compared with loss-cone analysis. Thereafter the case of time-dependent injection into a magnetic loop is addressed, and the results compared with previous analytic work on X and γ-ray delay times.

Key words: physical data and processes: scattering – Sun: corona – flares – X-rays and gamma-rays

1. Introduction

Partial trapping of electrons and protons in the solar corona is an inevitable consequence of field convergence between the coronal and chromospheric/photospheric parts of a coronal loop, which form a magnetic bottle (among such loops, the flare loop is the focus of this work). The 'trap-plus-precipitation' model is a popular model for the non-thermal flare component, and has been called upon to explain, for example, the time delay between hard X-rays and prompt γ-rays, e.g. Hulot et al. 1989 and Hulot et al. 1992 (hereafter HVT, HVCDK). Note, these delays have also been interpreted as being due to a two-step acceleration process, e.g. Bai (1982). In the trap-plus-precipitation model, particles are partially trapped in the convergent magnetic field of a coronal loop, with the trapped proportion and trapping timescale dependent on the energy and pitch-angle distribution of the injected population. In the absence of scattering, those particles with pitch-angle greater than a certain value defined by the ratio of field strengths (see Eq. 1) are trapped in the low-field region. In the presence of scattering, particles can enter the 'loss-cone' and leave the magnetic bottle. Particles of different energies are trapped for different times in the coronal bottle, and the various time delays observed in flare signatures are explained as being either due to the different emission peaks from of trapped and precipitating particles, or by precipitating particles which leave the magnetic bottle at different times, depending on their energies.

There is a considerable literature in existence on this problem. The idea of the magnetic trap in a solar context has been around since the 1960's (e.g. Takakura & Kai 1966). Melrose & Brown (1976) introduced the trap-plus-precipitation model in the context of a solar flare, taking into account the consequences of scattering in a coronal trap, whether by Coulomb collisions, or by some anomalous scattering mechanism. A number of more refined analytic treatments have appeared by e.g. MacKinnon (1988) and Alexander (1990), who both treated idealised forms of the weak diffusion (low scattering) limit, and by MacKinnon (1991) who treated the generalised problem (all scattering regimes), but used a Heaviside step function to approximate the loss-cone term (effectively the same as removing the spatial dependence of magnetic field convergence). McClements (1990a,b) used numerical and analytical techniques to study the case of an exponentially convergent magnetic field, but claimed that the results of his treatment would be insensitive to the dependence of the field convergence term on the spatial dimension. Precisely this dependence, amongst other factors, will here be investigated.

The aim of this paper is to use numerical simulations to study the evolution of electrons and protons trapped in a coronal loop. First of all, the 'loss-cone analysis' of particle evolution is compared with the results of numerical simulations with arbitrary scattering, in the case of gradual and abrupt field convergences. The method is then applied to the case of particles supposed to generate observable emission (hard X-rays and γ-rays), including Coulomb scattering and energy losses. The results of these simulations are compared with quantities such as the delay time calculated in the analytic work of HVT and the observed delay times reported in HVCDK.

2. Particle trapping in a coronal loop

Once they have been accelerated into a coronal loop, e.g. during a solar flare, energetic protons and electrons are influenced in their further progress by a number of factors which determine their lifetime and hence the time over which they emit observable radiation. Whilst non-thermal signatures are generated in the chromosphere, certain types of observed radiation are thought to be produced when particles are trapped in the solar corona (for example, long-lived γ-ray line emission produced

Table 1. Diffusion conditions

Type	Condition	Trap lifetime
Weak	$D_{\mu\mu} << \alpha_o^2 v/2L$	$1/D_{\mu\mu} = \tau_{sc}$
Intermediate	$D_{\mu\mu} \sim \alpha_o^2 v/2L$	τ_t/α_o^2
Strong	$D_{\mu\mu} >> \alpha_o^2 v/2L$	$> \tau_t/\alpha_o^2$

by trapped ions), and with the trap-plus-precipitation model it is possible to address the timing, sites of production and relative intensities of these signatures.

Most treatments of the effect of magnetic field convergence have relied on a simple description of particle losses from the trap, known as *loss-cone analysis*, as follows. If a particle's velocity vector has an angle to the magnetic field (pitch-angle) smaller than α_o where

$$\sin^2 \alpha_o = \frac{B_{min}}{B_{max}}, \tag{1}$$

B_{min} and B_{max} being the minimum and maximum magnetic fields in the trap, it may exit the trap. The cone in pitch-angle space of half-angle α_o is known as the 'loss-cone'. Particles may enter and leave the loss-cone by scattering, and whether they do, and how rapidly, depends on the diffusion coefficient. Based on this, there are three types of diffusion (e.g. Kennel 1969, Melrose 1986). Each case has associated with it a typical mean lifetime of a trapped particle, defined (in the case of steady and uniform injection into the trap) in the following way:-

$$\tau_{trap} = \frac{N}{Q} \tag{2}$$

(cf. Bespalov et al. 1991) where Q is the rate of injection (particles per second) into the trap and N is the number of trapped particles found once the population has stabilised at a constant value. Values for the trap lifetime, in the steady-state case, are given in Table 1 (e.g. Bespalov et al. 1991, MacKinnon, 1991).

In Table 1, v is the particle velocity and L the structure half-length. The transit time τ_t of particles in the loop is $\sim L/v$. In the weak case, particles scatter slowly towards the loss-cone, compared to the time they take to cross the structure, but once there they precipitate out almost instantaneously, and the loss-cone is almost empty. In the strong case particles are scattered quickly to the loss-cone compared with their structure-crossing timescale but once there may be scattered out again. The loss-cone in this case is almost full.

One problem with this treatment is that it is not always possible to define the loss-cone properly. The use of a single value for the loss-cone angle throughout a loop assumes that the magnetic field converges at a single position from the minimum to the maximum value. However if one suspects a magnetic field which varies along its entire length, the loss-cone is a varying function of particle position and also energy. This is not simple to treat analytically, so in this article the trapping and escape process is studied numerically, as described in the following section.

3. The transport equation

The motion of individual particles in a coronal loop is governed by various convective and diffusive influences - field convergence, energy loss, Coulomb scattering, etc. We shall initially (in Sect. 4) leave out any consideration of particle energy losses due to collisions or radiation, and concentrate on the effect of diffusion and magnetic field convergence. The equation describing the evolution of the particle distribution $f(S, \gamma, \mu, t)$ as a whole is the Fokker-Planck (F-P) equation, (including here the energy loss term, for future reference):

$$\frac{\partial f}{\partial t} + \mu v \frac{\partial f}{\partial S} - m_o D \frac{\partial}{\partial E}\left(\frac{f}{v}\right) - \frac{D}{v^3 \gamma^2} \frac{\partial}{\partial \mu}\left((1-\mu^2)\frac{\partial f}{\partial \mu}\right)$$

$$-\frac{v}{2}\frac{\partial}{\partial \mu}\left((1-\mu^2)\frac{dlnB}{dS}f\right) = s(S, \gamma, \mu, t), \tag{3}$$

where γ, v, μ, S, t are the particle energy in units of its rest-mass energy, speed, cosine of the particle pitch-angle, position along the field and time. Its rest mass is m_0, $D = D(S, \gamma)$ is the local pitch-angle diffusion coefficient, and $s(S, \gamma, \mu, t)$ is the source term for the injection of particles into the loop. Rather than seek an analytic solution to the F-P equation, the evolution of the distribution function will be modelled by simulating the motion of particles using a stochastic simulation. This technique allows one to study the the effect of scattering in combination with other effects such as magnetic field convergence. It is amply described in e.g. MacKinnon & Craig (1991), Achterberg & Krülls (1992), Fletcher & Brown (1995), Fletcher (1995). The reliability of the method in dealing with particle transport has been demonstrated by testing against restricted classes of numerical solutions. Briefly, a stochastic simulation is similar to a Monte-Carlo simulation in execution, in that the distribution function is built up by following the orbits of many individual test 'particles' under the influence of the relevant forces (in this case the magnetic mirror force and a scattering term). These are in general dependent on spatial and velocity co-ordinates of the test particle and so require to be continually updated as the calculation progresses. This is easily done in the stochastic simulation. The source term s is reflected in the initial distribution of injected particles, and the stochastic code models the post-injection transport of the particles.

The factor which makes the simulations particularly representative of real situations is that the diffusion term, often modelled in other Monte-Carlo treatments by a rather arbitrary amount of scattering, is calculated bearing in mind the physical nature of the scattering and of the particle distribution which results from it. So for example if one considers Coulomb scattering, the distribution of pitch-angle cosines which results from the scattering of an intially single pitch-angle distribution can be shown to be (almost) a Gaussian distribution with half-width proportional to the square root of the product of diffusion coefficient and time elapsed. (We say 'almost' because of course the pitch-angle cosine must always have magnitude less than one, whereas the Gaussian distribution extends to infinity.) So in the

simulation a representative value for the amount of pitch-angle scattering is at each timestep drawn from a Gaussian distribution and scaled by the square root of the product of the timestep used with the magnitude of the diffusion coefficient.

In a recent paper by Park & Petrosian (1996) the relative merits of stochastic simulations and finite difference methods in the solution of F-P equations were examined, for the case of Fermi-type acceleration. They found that, although reliable, the stochastic simulation method is not recommended for solving 1-d F-P equations being computationally expensive, and suffering from Poisson noise in cases where many decades in energy/intensity must be covered in a single simulation. The computational cost has indeed been found to be high when running simulations of particularly the weak-scattering cases, but we cover at the most two decades in energy in a single simulation. Also the framework for this type of solution was already in place, and it is conceptually simple. So although maybe the computations were not gone about in the best possible way, results obtained are satisfactory for the effort expended.

4. Particle trapping in converging magnetic fields - arbitrary scattering

4.1. A continuously convergent magnetic field

To get an idea of how representative or otherwise the loss-cone analysis is in general, the case of particles trapped in a magnetic field converging according to the following form,

$$B(s) = B_{min}(1 + s^2/h^2) \tag{4}$$

is studied, where s is the distance along a field line, h is the field scale length and B_{min} is the field minimum at the midpoint of the loop. In this case there will be a loss-cone whose angle varies continuously with position throughout the coronal loop.

There is no specified scattering mechanism, but diffusion is present, with coefficient scaled to the critical diffusion coefficient ν_c,

$$\nu_c = \frac{\alpha_o^2 c}{2L} \tag{5}$$

where c is the speed of light, so we are considering relativistic particles. The values $L = 10^9$cm and $\alpha_o^2 = 0.1$ are used. So $\nu_c = 1.5$. Let us calculate what loss-cone analysis predicts in these cases.
1) Weak scattering: $D_{\mu\mu} = 0.01\nu_c$. The prediction is $\tau_{esc} = 66.7$s
2) Intermediate scattering, $D_{\mu\mu} = \nu_c$. The prediction is $\tau_{esc} = 0.33$s
3) Strong scattering: $D_{\mu\mu} = 100\nu_c$. The prediction is $\tau_{esc} > 0.33s$

The time dependence of the total number of trapped particles in the strong and intermediate scattering cases are now studied numerically. Particles are injected at $z = 0$, the top of the loop, uniformly over a time period equal to twice the time interval over which the distribution is recorded. This ensures that there are no 'edge' effects. All particles are injected with
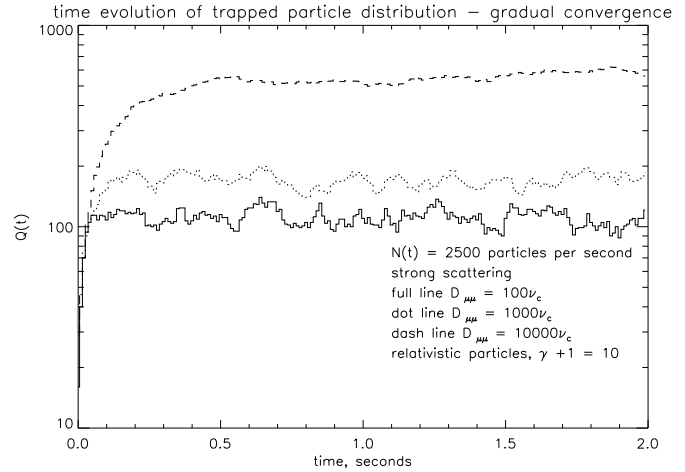
Fig. 1. The time evolution of the total population of trapped particles in the strong scattering case for a variety of values of the diffusion coefficient
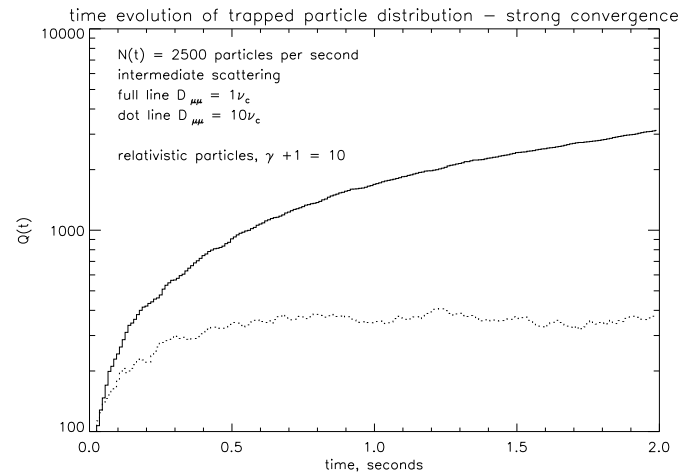

Fig. 2. As in Fig. 1, but for intermediate scattering

the same energy of $\gamma + 1 = 10$. In these, and all following simulations, the input distribution is uniform over particle pitch angle, which, if azimuthal symmetry is assumed, corresponds in 3-d to a strong degree of beaming along the magnetic field (equal particle numbers in equal angular intervals $d\theta$, but the surface area on a sphere subtended by $d\theta$ at θ varies as $1/\sin\theta$, therefore surface density increases towards small θ - i.e., the beam axis).

In the weak scattering case, run-times are prohibitively long, and the use of a finite-difference approach is advocated. The results of the simulations for the strong scattering case are shown in Fig. 1.

From Fig. 1, in the simulated strong scattering cases the lifetimes derived for $D_{\mu\mu} = 100$, 1000 and 10000 ν_c are 0.044, 0.072 and > 0.24s respectively. The lifetimes thus show the correct variation with increasing diffusion coefficient but are well below the minimum theoretical value of 0.33s. This could be because the trapped particles are not executing truly random walks, meaning that they escape faster than predicted. Alter-
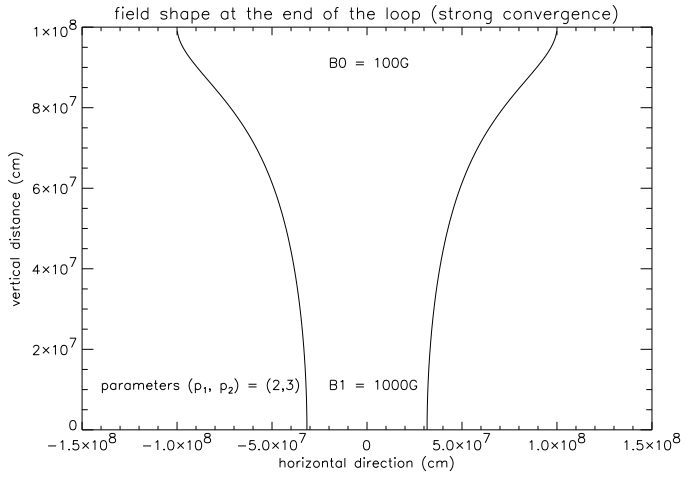
Fig. 3. The shape of the field convergence used in the strong convergence calculations. Only the bottom 10^8 cm is shown - the remainder of the loop has a constant magnetic field of 100G

natively, since the magnetic field structure is not one of abrupt convergence, the loss-cone description is not strictly applicable. This latter possibility can be tested by changing the field shape, which is done in the following Subsection.

Figure 2 shows the intermediate scattering case. The lifetimes simulations for $D_{\mu\mu} = 1$ and $10\nu_c$ are > 1.5s and 0.25s respectively. These are comparable to the theoretical value of 0.33s.

4.2. An abruptly convergent magnetic field

We use this time a magnetic field shape which more closely mimics the ideal case of instantaneous strong convergence. The field equation is

$$B_r(S) = B_{min} + \frac{(B_{max} - B_{min})}{(p_2 - p_1)}[p_2 x^{p_1} - p_1 x^{p_2}] \qquad (6)$$

(MacKinnon & Brown 1990) where (p_1, p_2) are parameters controlling respectively the convergence strength and position and x is the scaled distance parameter s/L. We utilise parameters $(p_1, p_2) = (2, 3)$ corresponding to a relatively sharp convergence near the tube ends. The field shape at the bottom of the loop is shown in Fig. 3. The field strengths at the top and bottom of the tube are the same as in Sect. 4.1, but the nature and position of convergence has been altered. In this case, the uniform field region has a half-length of 10^9cm, added onto which is the convergence region, 2×10^8 cm. The predicted lifetime is thus > 0.4s in the strong scattering case. As will be seen in Fig. 4 below, the agreement between the loss-cone predictions and the simulation results is somewhat better in this case, with lifetimes of 0.58s, 0.46s and 0.50s for 100, 1000 and 10000 ν_c respectively. In the calculation performed for the intermediate scattering case, lifetimes of 0.8, 1.0 and 1.2 s for 10, 1, and 0.1 ν_c are determined, which should be compared with the analytic value of 0.4s.
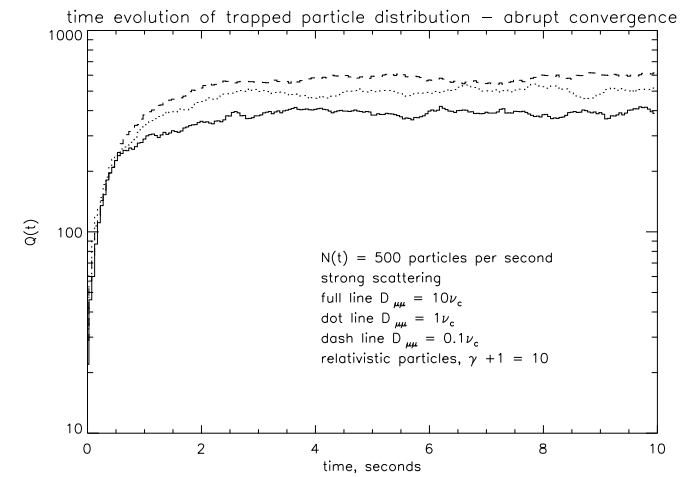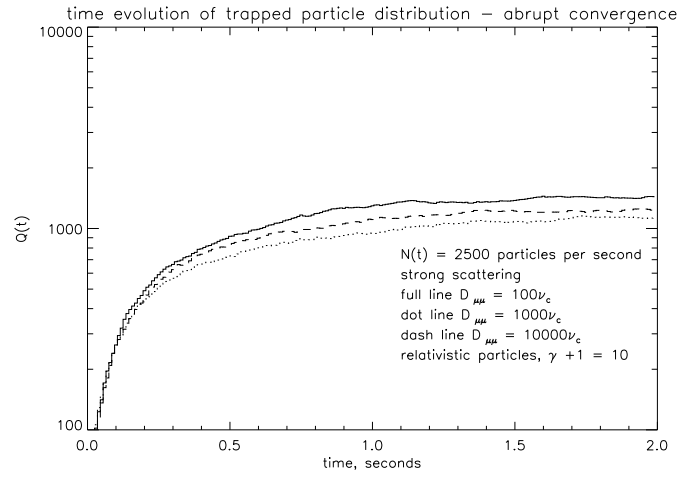
Fig. 4. As Figs. 1 and 2 but for the case of abrupt magnetic field convergence as shown in Fig. 3.

The indication from this series of simulations is that not only the amount but the form of magnetic field convergence has an important effect on the escape timescales of particles in the loop, at least in the strong and intermediate cases investigated. There can be more than an order of magnitude difference between the timescale predicted by loss-cone analysis and the simulation results, depending on the shape of the field and the value of the diffusion coefficient. In the case of continuous convergence, the strong diffusion escape timescales were considerably lower than those predicted by the loss-cone analysis, whilst in the abrupt convergence case they were in better agreement. This suggests that the weak field gradient near the base of the loop in the gradual convergence case is not enough to kick the rapidly scattered particles near the base of the loop back into the body of the loop before they diffuse out of the structure. The result of field-shape variations in the intermediate scattering case is also consistent with this, though the effect is not so pronounced. Whether or not a particle will precipitate in this case is not so much determined by diffusion at the base of the coronal

structure, but by its initial pitch-angle compared to that which would allow it to escape in the complete absence of scattering.

These results suggest that a degree of caution should be exercised in using loss-cone analysis for the analysis of data in the trap-plus-precipitation model, certainly in the strong and to a lesser extent in the intermediate scattering regimes. Such a conclusion is important in the context of the analysis of γ-ray/HXR delays, where strong scattering is invoked as a trapping mechanism.

5. The time and energy distribution of trapped protons

It is of interest to see how trapping behaves as a function of energy, since this is the basis for the analysis of delays in X and γ-ray signatures. To this end, we study the evolution of a distribution of protons, which we model as a power-law in energy. Protons are responsible for prompt γ-ray emission in impulsive solar flares. Note that in what is to come we are concerned with the time-dependent case, thus the loss-cone analysis is inapplicable anyway. In the simulations of this section, the ratio $\alpha_o^2/L = 10^{-10}\text{cm}^{-1}$, the injection time profile is symmetric and triangular, with total duration 10s, the injected proton energy distribution is a power-law in flux, with index -3.5, being a typical solar flare power-law spectrum (a cutoff is imposed at 10MeV). The injection is intially isotropic. The field convergence is of the gradual nature used in Sect. 4.1.
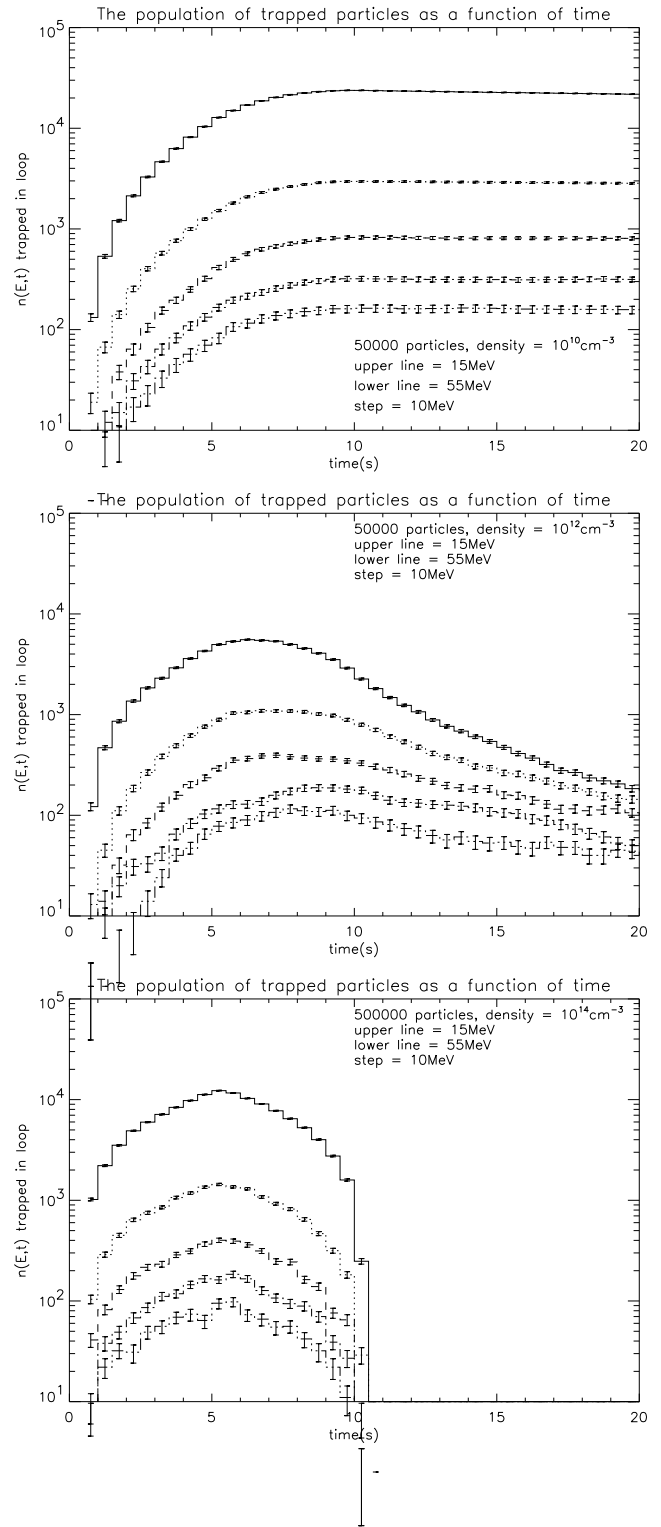
5.1. Coulomb diffusion

In the following simulations we include the effects of field convergence, scattering and energy loss due to Coulomb collisions, which are taken to be the only source of particle diffusion, thus relating the scattering regime to the loop density. For these non-relativistic protons, the diffusion coefficient (as used in Eq. 2) is

$$D_{\mu\mu,p} = \left(\frac{m_e}{m_p}\right)D_{\mu\mu,e} = \left(\frac{m_e}{m_p}\right)\frac{8\pi\Lambda n_l e^4}{m_e^2 v^3}, \tag{7}$$

where n_l is the local electron density (assuming completely ionised hydrogen) m_e, m_p are the electron and proton rest-masses, and Λ is the Coulomb logarithm. In the loss-cone description, with parameters $L = 10^9\text{cm}$, $\alpha_o^2 = 0.1$ and $v \sim 1 \times 10^{10}\text{cms}^{-1}$, the value of the critical diffusion coefficient ν_c is 0.5, so a typical solar flare density in the range 10^{9-12}cm^{-3} places us in the weak diffusion limit for protons, and 10^{13-15} cm^{-3} corresponds to intermediate to strong diffusion. Observationally there is no evidence for loop densities above a few $\times10^{12}\text{cm}^{-3}$ but this strong scattering case is included for the sake of illustration.

The simulation parameters have been chosen to enable comparison between the timing results of the present method with those of HVT and HVCDK (though more particularly in the next section where we consider also non-Coulomb diffusion).

Some time profiles of the trapped particle distribution as a function of energy, in a number of scattering regimes, are presented in Fig. 5.

Fig. 5. The time evolution of a distribution of trapped protons shown as a function of energy for three different density values, in the weak, intermediate and strong diffusion cases. All scattering is due to Coulomb collisions

1) Weak scattering: Fig. 5, top panel - at a density of 10^{10}cm^{-3} the particle distribution shows a fairly rapid rise to a maximum number density at a few seconds after the injection maximum, followed by a slow decay. The decay time constant increases with increasing energy - high energy particles are trapped with greater efficiency than low energy particles (note that the decay is due to trap losses rather than Coulomb losses - the timescale for the latter is far longer than the interval shown). On average the maximum of the distribution function is 4-5 seconds after the time of the injection peak (seen if one expands the n(t) axis). Statistics are good in this case because trapping in the weak scattering regime is efficient and many particles remain in the trap. The profile remains rather smooth up to 50 MeV or so.

2) Intermediate scattering: Fig. 5, middle panel - at a density of 10^{12}cm^{-3} we are in the weak/intermediate scattering regime. The form of the profile is very similar to the above case, but the time difference has decreased to 3-4 seconds. The decay here is due mostly to Coulomb losses which at this density and typical energies have a characteristic timescale of a few seconds. The values of HVT show delays of 2.5-1.5s.

3)Strong scattering: Fig. 5, bottom panel - at 10^{14}cm^{-3} we are in the intermediate/strong scattering regime, and here the time profile is far more symmetric around the peak injection time, with much smaller time differences - less than a second.

It is difficult in most cases to measure from the graphs the difference between injection maximum and population maximum to better than 0.5-1s. There is often no obvious 'peak' to the population density at a given energy. Of course, the numerical approach used here means that there may well be an overlap in the error bars on adjacent bins, thus an effective spreading in the position of the maximum which can be found from the histogram, dependent on the number of particles in the simulation, but even without this confusion the slow population decay leads to a very broad maximum. In effect this means that for low trap densities ($\lesssim 10^{12}$cm^{-3}) the loss of protons from a magnetic trap in the continually convergent field is rather slow and steady. It is thus not possible to generate impulsive emission in this low density case unless an alternative form of diffusion is invoked. However, such long timescale trapping is recognised as possibly explaining long duration γ-ray events, e.g. Vilmer (1994), Trottet et al. (1993) - if appropriate twist can be imposed on the loop to prevent cross-field leakage (cf. Lau et al. 1993).

The time difference between injection and maximum in trapped populations are derived for densities 10^{10}, 10^{11} and 10^{12} cm^{-3} and shown in Fig. 6. The points are at $T_{max}(E)-T_{max,inj}$ (s) where $T_{max}(E)$ is the time corresponding to the bin with the maximum counts at a given energy E and $T_{max,inj}$ is the time of the maximum of particle injections, 5s. The error is given by spread in times over which the $\sqrt{N}$ error on the maximum bin overlaps the tops of the surrounding bins. At the lowest densities shown the delay is around 5 seconds, with a slight upwards trend. At 10^{11} cm^{-3} the delay calculated is 2 - 5s, with the difference increasing with increasing energy. At 10^{10}cm^{-3}, HVT found delays of 3 to 1.5s, falling with particle energy - inconsistent with the present simulations. At 10^{11}cm^{-3} they found delays of 2.5-1.5s, falling with particle energy whilst at 10^{12}cm^{-3} the de-
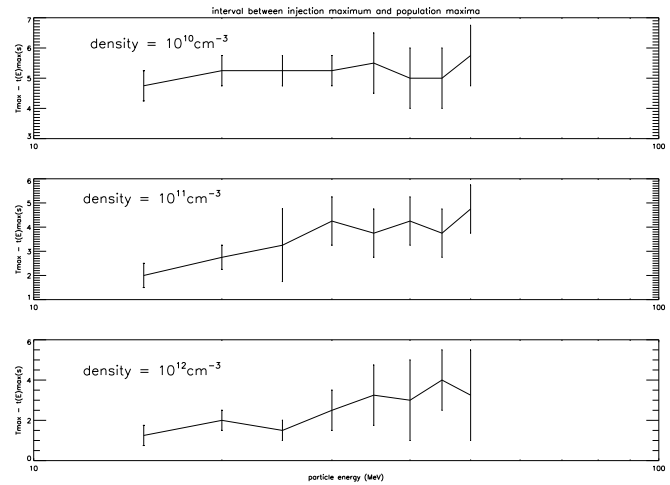
Fig. 6. The time differences calculated numerically for three density cases.

lays were from $\sim 1-1.5$s, peaking around 40 MeV. The present calculations agree with the results of HVT in that they demonstrate a delay which is on average decreasing with increasing local density, however the size of the delay and the variation with energy found here for 10^{-10}cm^{-1}, is more consistent with the results of HVT for the case of $\alpha_o^2/L = 10^{-11}$cm^{-1} - i.e. a longer loop or a narrower loss-cone (stronger field convergence). In other words, the case of a gradual field convergence plus the inclusion of the full scattering treatment gives better trapping than does the mean-scattering treatment with an abrupt convergence. This is consistent with the fact that in a mean-scattering treatment the process of diffusion is poorly represented (underestimated), especially for particles with high pitch-angles.

The effect of the gradual field convergence may also play a role in explaining the difference between trapping times found in this and the previous work. In the intermediate case ($D_{\mu\mu} = \nu_c$ in Sects. 4.1 and 4.2) a gradually convergent field appeared to improve the trapping time compared with an abruptly convergent field. This would also contribute to the discrepancy just found between these results and those of HVT, at least around the intermediate scattering region.

We have not been able to perform these simulations for low loop density values, since they take a prohibitively long time to run. But following the trends shown it is expected that the time difference would in be greater than 5 seconds.

6. Gamma-ray/hard X-ray time delays

In this section the time delays are calculated between the peak emission of hard X-ray and γ-ray emission for comparison with the work of HVCDK. These authors found that the flux of 4.1-6.4 MeV γ-rays was, in a number of flares, delayed with respect to 154-236 keV hard X-rays. This they explained with a magnetic trap-plus-precipitation model, in which protons, which generate the γ-ray emission, are well trapped in the coronal loop, and the peak of the time profile of precipitating protons

is delayed with respect to that of precipitating electrons, which generate the HXR flux. We shall model this situation in the following section.

Since HXR radiation can only be produced by electrons of energy above the energy of the radiation, the time of the maximum in the 150 keV hard X-ray flux is associated with the time of maximum population of electrons of energy greater than 150 keV (precipitating *and* trapped, depending also on the density of the medium in which they generate radiation). Similarly, for γ-ray emission in the observed energy band, dominated by ^{12}C and ^{16}C de-excitation lines, we look at protons of $\gtrsim$ 10MeV. Both of these channels are of a prompt nature, so there is no delay between the interaction of fast particle and atom and the emission of the observable radiation. The maximum in the γ-ray emission thus occurs at the time of maximum proton population. Therefore the difference in time between the maxima in both particle populations gives a fair idea of the HXR/γ-ray delay which would be observed. The test case chosen is the time delay observed between γ-ray and HXR fluxes in the short impulsive flare of 7 June 1980, studied by HVCDK. In this flare the γ-ray profile in the band integrated over 4.1 - 6.4 MeV delayed by about 2 seconds with respect to the hard X-ray profile integrated over 154 - 236 keV.

In modelling this process the conditions used are the same as those used by HVCDK. The injection has a parabolic time profile with total duration 5 seconds. The injection, for both protons and electrons, has the form of a power-law in flux with index -3.0, and the injection profiles are simultaneous. The case of Coulomb collisions, with and without an arbitrary strong (lossless) scatterer is studied. HVCDK also invoked an arbitrary source of strong diffusion, identifying it with Alfvèn turbulence, or whistlers. We make no assumptions about the origin of this extra term, defining only its angular form and magnitude. The abrupt field convergence of MacKinnon & Brown (1990) is used, and $\alpha_o^2/L = 1.0 \times 10^{-10}$cm^{-1}.

A single value for chromospheric density of 10^{15}cm^2 is used, and particles are considered to have precipitated as soon as they exit the loop. (Although this means that one may in certain cases underestimate the time of maximum emission, by neglecting the transit time to dense regions, the difference in time would be less than our bin resolution - the energy loss time for 30MeV protons in a density of 10^{15}cm^{-3} is less than a tenth of a second). We look at coronal densities of 10^{10}, 10^{12} and 10^{14} cm^{-3}, with the latter very high density case again being included for the purposes of illustration.

Electrons: First of all the case is presented in which, in addition to Coulomb scattering, we use an arbitrary strong scattering source with $D_{\mu\mu,e} = 10^4\nu_c$. In fact, at all the densities studied, Coulomb collisions alone would provide a source of strong diffusion for electrons, and no additional scattering source would be needed to trap them quite efficiently. Results are shown for three different density values in Fig. 7.

The histograms shown are the sum of the trapped and precipitating populations, each scaled by the local density and normalised to each other and the chromospheric density. This ac-
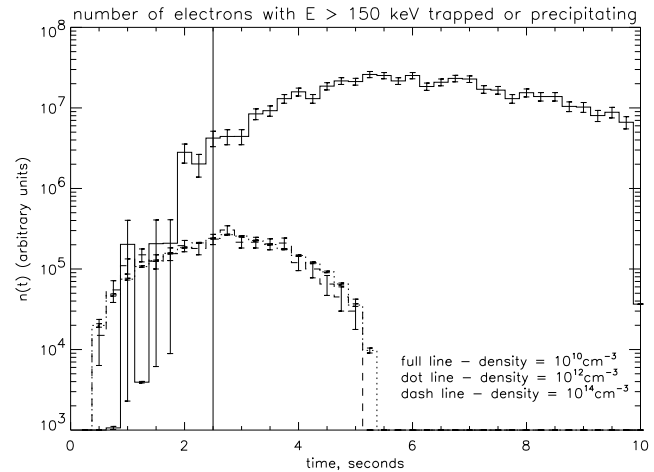
Fig. 7. The time profiles of trapped and precipitating electrons of energy above 150keV, for an arbitrary strong scatterer plus Coulomb collisions in various density loops. The vertical line marks the time of maximum injection (2.5s).

counts for the fact that even if the majority of electrons are trapped, the minority that precipitate would generate intense HXR emission by virtue of the fact that they enter a dense chromosphere.

At the higher densities of 10^{12} and 10^{14}cm^{-3}, all particles in the simulation are trapped, and the entire population loses its energy in the loop, consistent with what is found by HVCDK. In both cases the population peaks at almost the same time as the injection peaks. At the highest density case, particles lose their energy very rapidly, and the number recorded in the loop is in consequence very small. At the lower density of 10^{10}cm^{-3}, most of what is seen is the scaled population of precipitating particles, but the trapped population peaks at the same time. The population peak is delayed with respect to the injection peak by 3.25 ± 0.5 seconds, which is considerably longer than was found under the same conditions by HVCDK. As the presence of the strong diffusion term places us firmly in the strong scattering regime, this discrepancy is indicative of the underestimation of the scattering efficiency which comes of the use of a mean-scattering treatment by HVCDK.

Next the case of electrons without the presence of the additional strong scatterer is examined. In this case, more electrons should be able to precipitate. Results of these simulations are shown in Fig. 8.

At 10^{14}cm^{-3}, coronal emission dominates - no electrons get to the chromosphere, because of a combination of high Coulomb losses and effective Coulomb scattering leading to good trapping. At 10^{12} cm^{-3} diffusion and energy loss of electrons by Coulomb scattering is relatively strong and there is practically no delay to be seen between the time of maximum of injection and population maximum. However at $n = 10^{10}$cm^{-3}, scattering is quite weak and delay appears, corresponding to particles taking a while to reach the loss-cone. So it is no surprise to see a delay between injection maximum and population maxi-
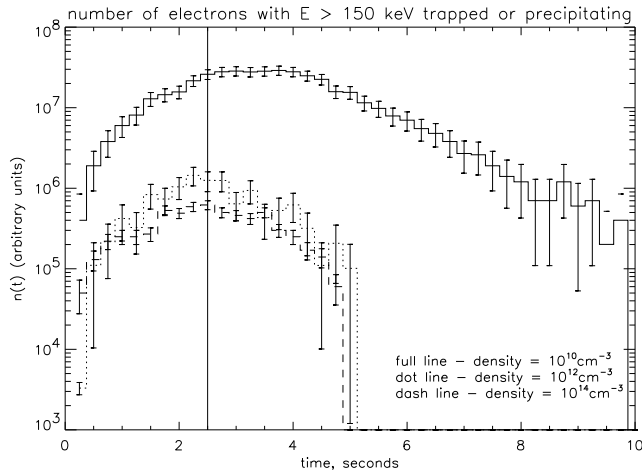
Fig. 8. The time profiles of trapped and precipitating electrons with energy above 150keV, for Coulomb collisions in various density loops. The vertical line shows the time of maximum injection (2.5s).

mum. This delay is more-or-less the same in both the trapped and precipitating populations, but emission from the precipitating population dominates. The delay is 1.25 ± 0.75s; smaller than the delay found at the same density in the previous investigation, when electrons were well trapped by strong scattering in the loop. This difference just depends on the choices for the strength of the strong diffusion term, and the loop density.

In summary, it is found that, the absence or presence of an additional strong scattering term for electrons does not affect the timing of the electron population maxima, except at 10^{10}cm^{-3}, where the delay is longer if a strong scattering source is included, but that, with the assumption of a chromospheric density of 10^{15}cm^{-3}, the ratio of emission from trapped and precipitated electrons does change - especially around 10^{12}cm^{-3}.

Protons: Proton simulations have been performed for a variety of loop densities and arbitrary diffusion coefficients. In the case of protons, we always assume the combination of Coulomb and arbitrary strong sources, used by HVCDK. One example case is presented in Fig. 9. In this case the loop density is 10^{12}cm^{-3}, and the diffusion coefficient $D_{\mu\mu,p} = 10^4\nu_c$. Summaries of the proton-electron time delays found by running many simulations are presented in Tables 2 and 3. Recall that for the simulations presented in Table 2, only a single value of the strong scattering coefficient for electrons (= $10^4\nu_c$) was investigated, whereas in both cases the proton strong scatterer ranges in strength.

As in HVCDK, delays of the order of 2s can be found, but for different loop conditions. What is immediately obvious from Table 2 is than in the present simulations, such delays do not occur if a strong diffusion source is present for *both* electrons and protons. In such a case, the electron population peaks around the same time as the proton population. The delays of order 2s observed in the June 7 1980 event were interpreted by HVCDK as originating from a simultaneous injection of electrons and protons into a trap of density $\sim 5 \times 10^{12}$cm^{-3}, in the pres-
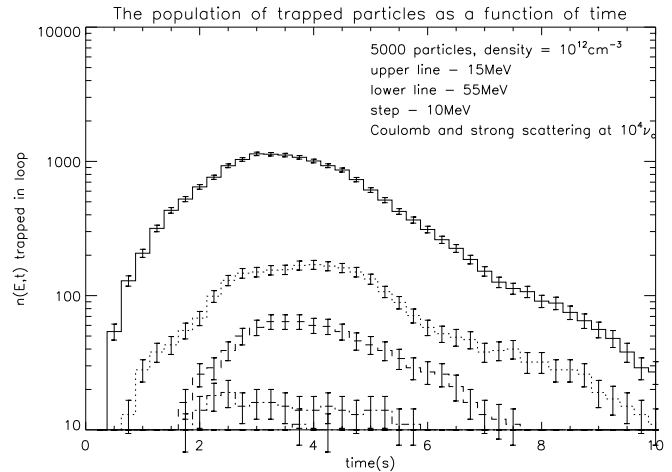
Fig. 9. The time profile of the trapped proton population in the case of an arbitrary strong diffusion mechanism dominating

Table 2. 15 MeV Proton - 150 keV Electron maximum time delays (seconds), in the case of arbitrary strong scatterers for protons and electrons.

Loop density cm^{-3}	10^{10}	10^{12}	10^{14}
$D_{\mu\mu,p}$			
$10^2\nu_c$	0.25	0.25	0.0
$10^3\nu_c$	0.0	0.0	0.0
$10^4\nu_c$	0.0	0.0	0.0

Table 3. 15 MeV Proton - 150 keV Electron maximum time delays (seconds), in the case of an arbitrary strong scatterer for protons only.

Loop density cm^{-3}	10^{10}	10^{12}	10^{14}
$D_{\mu\mu,p}$			
$10^2\nu_c$	2.25	0.75	0.0
$10^3\nu_c$	2.0	0.5	0.0
$10^4\nu_c$	2.0	0.5	0.0

ence of a strong diffusion source for both electrons and protons. But in the case of electrons and protons with the additional strong diffusion source, it should be expected that the delays between electron and proton maxima are always zero - at the particle energies of interest the strongest source of scattering is always provided by the additional strong diffusion term, and the Coulomb stopping lengths for both species at the energies chosen ($\sim$ 150 keV electrons and $\sim$ 15 MeV protons) are approximately equal. The particles should thus have very similar trapping and loss timescales.

The alternative scenarios giving positive delays of the protons with respect to the electrons are as follows:
1) only Coulomb collisions present - in which case at 10^{10-12}cm^{-3} protons would be confined to the loop for long periods (cf. Sect 5.1) whilst electrons are precipitated immediately or after about 1.25 seconds (from the simulations presented in Fig. 8). However, this would not give a proton 'peak', because of the long time-constants for proton trapping.
2) Protons are subjected to strong scattering whilst electrons

only scatter under the influence of Coulomb collisions. This second case has been investigated and the results in Table 3 indicate that a time delay of the order of 2 seconds *can* be found for a simultaneous injection of protons and electrons, at 10^{10}cm^{-3}. Even if we interpret this as the leaky trap case of HVCDK, a lower value of the trap density is found in these simulations. In the present work, at a density of $\gtrsim 10^{12}$cm^{-3}, delays are less than a second.

We conclude from these simulations that the observed delays between electron and proton signatures cannot be explained if there is strong scattering present which affects both electrons and protons (at least if the strong scattering is assumed arbitrarily to have the same timescale for both species). If protons are strongly scattered but electrons are not, the delays do appear. This indicates also that if one could be more specific about sources of scattering, and move away from the simple statement that diffusion is strong, the observed delays could perhaps be explained by the presence of particular mechanisms other than Coulomb scattering for both protons and electrons. But evidently, with the extra freedom which would be introduced in this way, more modelling would be necessary.

7. Discussion and conclusions

It has been shown using numerical simulations of the transport of energetic particles in a coronal magnetic bottle that the loss-cone analysis of particle trapping and precipitation does not always provide an adequate description of the physical situation. In particular it has been demonstrated that escape timescales calculated using numerical simulations vary considerably from those predicted in the loss-cone analysis, if the field *shape* varies from the abrupt convergence case, which is the only geometry to which loss-cone analysis can be safely applied. In solar physics, therefore, loss-cone analysis should be applied with caution, particularly to strong scattering cases. If one has evidence for a considerable field convergence in the corona (e.g. from Yohkoh SXT images) then particle trapping and precipitation ought to be modelled by a numerical technique in which the field shape enters, such as we have presented here. This will be important in the analysis of CGRO, Yohkoh HXT time and time-of-flight data. The application of this analysis to any such data is yet to be attempted

Delay times have been calculated, for comparison with previous work by HVT and HVCDK. Firstly, the time difference between the injection maximum and the population maximum of trapped protons was calculated, and discrepancy found of as much as 3s over a 10s injection; in explaining delay observations of a few seconds this can be quite significant. The field used in these calculations was of the gradually varying type, so one would expect this to give the biggest differences from the theoretical treatment, which postulates an instantaneously varying field. Further calculations were carried out of the delay in the population maxima of protons generating γ-rays and electrons emitting hard X-rays. It was found that with the parameters used by HVT, although delays of around 2 seconds could be generated by trapping, these delays were not present in the case where both electrons and protons are scattered by an arbitrary strong source. In the case where protons are subject to strong and Coulomb diffusion terms, whereas electrons only suffer Coulomb collisions, a delay of around 2 seconds was found, but this occurred at a lower density than was found by HVCDK. The discrepancies between the current and the previous work can be, at least qualitatively, attributed to the difference between a mean-scattering and full scattering treatment of particle evolution, the former tending to underestimate the effect of diffusion.

References

Achterberg A., Krülls W., 1992, A&A 265, L13
Alexander D. 1990, A&A 235, 431
Bai T., 1982. In Gamma-Ray Transients and Related Astrophysical Phenomena, Vol 77, A.I.P., Lingenfelter R.E., Hudson H.S., Worall D.M. (eds), New York, p. 409
Bespalov P.A., Zaitsev V.V., Stepanov A.V. 1991, ApJ 374, 369
Fletcher L., 1995, A&A 303, L9
Fletcher L., Brown J.C., 1995, A&A 296, 260
Hulot E., Vilmer N., Trottet G., 1989, A&A 213, 383
Hulot E., Vilmer N., Chupp E.L., Dennis B.R., Kane S.R., 1992, A&A 256, 273
Kennel C.F., 1969, Rev. Geophys. 7, 379
Lau Y.-T., Northrop T.G., Finn J.M., 1993, Ap.J. 414, 908
MacKinnon A.L., 1988, A&A 194, 279
MacKinnon A.L., 1991, A&A 242, 256
MacKinnon A.L., Brown J.C., 1990, A&A 232, 544
MacKinnon A.L., Craig I.J.D., 1991., A&A 251, 693
McClements K.G., 1990a, A&A 230, 213
McClements K.G., 1990b, A&A 234, 487
Melrose D.B., Brown J.C., 1976, MNRAS 176, 15
Melrose D.B., 1986, 'Instabilities in Space and Laboratory Plasmas' p237, C.U.P
Park B.T., Petrosian V., 1996, ApJS 103, 255
Takakura T., Kai K., 1966, PASJ 18, 57
Trottet G., Vilmer N., Barat C., Dezalay J.P., Talon R., et al., 1993, A&AS, 97, 337
Vilmer N., 1987, Sol.Phys. 111, 207
Vilmer N., 1994, ApJS 90, 611